Modeling of CO_2 splitting in a microwave plasma : how to improve the conversion and energy efficiency

Modeling of CO_2 Splitting in a Microwave Plasma: How to Improve the Conversion and Energy Efficiency?

Antonin Berthelot and **Annemie Bogaerts***
Department of Chemistry, Research group PLASMANT,
University of Antwerp, Universiteitsplein 1, 2610 Antwerp, Belgium
E-mail : annemie.bogaerts@uantwerpen.be

Abstract

Microwave plasmas are one of the most promising techniques for CO_2 conversion into value-added chemicals and fuels, since they are very energy-efficient. Nevertheless, experiments show that this high energy efficiency is only reached at low pressures, and significantly drops towards atmospheric pressure, which is a clear limitation for industrial applications. In this paper, we use a zero-dimensional reaction kinetics model to simulate a CO_2 microwave plasma in a pressure range from 50 mbar to 1 bar, in order to evaluate the reasons for this decrease in energy efficiency at atmospheric pressure. The code includes a detailed description of the vibrational kinetics of CO_2, CO and O_2 as well as the energy exchanges between them, because the vibrational kinetics is known to be crucial for energy efficient CO_2 splitting. First, we use a self-consistent gas temperature calculation in order to assess the key performance indicators for CO_2 splitting, i.e., the CO_2 conversion and corresponding energy efficiency. Our results indicate that lower pressures and higher power densities lead to more vibrational excitation, which is beneficial for the conversion. We also demonstrate the key role of the gas temperature. The model predicts the highest conversion and energy efficiencies at pressures around 300 mbar, which is in agreement with experiments from literature. We also show the beneficial aspect of fast gas cooling in the afterglow at high pressure. In a second step, we study in more detail the effects of pressure, gas temperature and power density on the vibrational distribution function and on the dissociation and recombination mechanisms of CO_2, which define the CO_2 splitting efficiency. This study allows us to identify the limiting factors of CO_2 conversion and to propose potential solutions to improve the process.

1. Introduction

The vast majority of the energy used on our planet originates from the combustion of fossil fuels, thus emitting CO_2, a greenhouse gas contributing to the increase of global warming[1]. One of the proposed strategies to reduce the CO_2 concentration is its conversion into value-added chemicals, such as CO[2]. Low temperature plasmas have been shown to be an energy-efficient way to dissociate CO_2 [3], with reported energy efficiencies up to 90% in conditions of supersonic gas flow in a microwave discharge[4]. Recently, new efforts have been made to study the possible industrial applications of CO_2 conversion

using different plasma setups: dielectric barrier discharges (DBDs)[5–8], gliding arc discharges[9,10] and microwave (MW) plasmas[11–16].

These discharges have the interesting property to be in non-equilibrium: the electrons typically have much higher translational temperature than the heavy particles (neutral and ions). Such non-equilibrium behavior enables endothermic reactions, such as CO_2 dissociation, to occur without requiring an increase of the gas temperature, thus saving energy. This is especially relevant in the frame of energy efficient processes. In particular, the high energy efficiency obtained in MW and gliding arc discharges is generally attributed to vibrational excitation. At the relatively low electron temperature characteristic for these type of discharges, i.e., between 1 and 2 eV, vibrational excitation is one of the main mechanisms through which electrons transfer their energy to the CO_2 molecules, leading to dissociation[3].

While it was reported that the best energy efficiencies in MW plasmas are obtained between 100 and 200mbar[3], it would be particularly interesting for industrial application to use a process working at atmospheric pressure. Indeed, the energy efficiencies usually reported in the literature only take into account the energy consumed by the plasma and not the total energy consumption. In a real chemical installation, different extra energy costs have to be taken into account and the energy consumption of a vacuum installation is typically not negligible.

In order to achieve better energy efficiencies on industrial scale devices, it is necessary to obtain a better understanding of the different dissociation and recombination mechanisms of CO_2, and particularly the role of the vibrational kinetics[17]. In 1967, Treanor et al.[18] derived an analytical expression for the population of the different vibrational levels in an anharmonic oscillator, such as CO_2, excluding the influence of dissociation and VT transfers. It was shown that it is possible to obtain large populations of highly-excited vibrational levels under conditions of low gas temperature and large vibrational energy, i.e. strong non-equilibrium conditions.

Computer modelling is particularly useful to provide detailed information on processes that are difficult, or even impossible, to measure experimentally. Within our group we developed a chemical kinetics model to investigate in detail the plasma chemistry of CO_2 dissociation in a DBD and a MW plasma[17,19–21]. While in a DBD plasma the CO_2 splitting mainly proceeds by electron impact dissociation, as revealed by several models[17,20,22], in a MW plasma the vibrational kinetics are found to play a dominant role. In particular, we studied the role of the reaction $CO_2 + O \rightarrow CO + O_2$ on the energy efficiency of CO_2 conversion in a MW plasma, at a pressure of 100 Torr[19] as well as the effect of its activation energy. The effect of adding N_2 to CO_2 on the dissociation mechanisms in a MW plasma was also investigated[23]. More recently, the influence of the dissociation cross section by electron impact was studied[24,25], advising the use of the Phelps 7 eV cross section[26] . In this study[24] we observed, among others, that the role of electron impact dissociation in a MW plasma diminishes with increasing pressure. Pietanza et al. also investigated the importance of the electron energy distribution function (EEDF) and of vibrational excitation on the dissociation of CO_2[27–29]. Solving the Boltzmann equation, the authors showed that the vibrational temperature has a large influence on the relative contribution of the different dissociation processes.

In spite of these investigations, there is still a lack of detailed understanding of the most important plasma parameters in a MW discharge, such as the pressure, the power density and the gas temperature. These parameters have a strong influence on the conversion and energy efficiency in a MW plasma and are thus particularly relevant to gain a better understanding of the underlying mechanisms, and to improve the process of CO_2 conversion.

The aim of the present research is thus to provide more insights in the relevant dissociation and recombination mechanisms of CO_2 in a MW discharge, in a wide range of conditions of pressure, power deposition and gas temperature. In particular, we will focus on the role of vibrational excitation, because of its importance for energy efficient CO_2 splitting. The paper is organized as follows. In part 2, we present the equations solved by the model, the chemistry included and the most important parameters calculated by the model. The results section, part 3, is divided into two main parts. First, we present a self-consistent gas temperature calculation and we investigate the conversion and energy efficiency in a wide range of discharge conditions (part 3.1). Then, we consider a simplified case with a fixed gas temperature to better understand the effect of vibrational excitation (part 3.2) and of the relative importance of the different dissociation and recombination mechanisms for CO_2 splitting (part 3.3), making the link with the results shown in part 3.1. Furthermore, in part 3.4, we propose some possible ways to improve the experiments based on all these findings. Finally, conclusions are given in section 4.

2. Model description

2.1 Equations solved by the model

We developed a zero-dimensional chemical kinetics model using the code ZDPlasKin[30]. This model describes the plasma chemistry in a CO_2 non-equilibrium discharge. In order to account for the axial variation of the various plasma quantities, the model follows a volume moving through a cylindrical discharge tube and passing through the plasma region. The 0D model only allows following the axial variation of the plasma quantities and considers a radially homogeneous plasma. Note that the purpose of this study is to understand the effect of the different parameters on the plasma in a general (surfatron) MW discharge, rather than in a specific setup, in order to make it of broad interest. The plasma is formed using microwaves in a quartz cylindrical discharge tube (see Figure 1), cooled to room temperature.

The considered volume moves at a velocity v calculated from the conservation of the mass flow rate:

$$v = \frac{Q_m}{\rho A} \qquad (1)$$

Where Q_m is the mass flow rate, $\rho = \sum_s n_s M_s$ is the gas mass density and $A = \pi R^2$ is the tube cross section area. n_s is the number density of the species s, M_s is the mass of species s and R is the tube radius.

By means of this velocity, the time-dependence of the 0D chemical kinetics model can be converted into an axial-dependence throughout the discharge tube. Therefore, it is possible to express the power deposition as a function of z, the axial coordinate (see Figure 1). We consider a triangular power deposition density profile given by:

$$Q_{MW}(z) = \begin{cases} \left(1 - \left|\frac{z - (z_p + L/2)}{L/2}\right|\right) P_{max} & if\ z_p \le z \le z_p + L \\ 0 & otherwise \end{cases} \qquad (2)$$

L is the plasma length, z_p is the axial coordinate at which the plasma starts and Q_{max} is the maximum power deposition density (see Figure 1). The mean power deposition density is then $Q_{max}/2$. This expression of the power density is used in part 3.1. In parts 3.2 and 3.3, we simply define a fixed power density for a given time, so that the absorbed energy matches the required specific energy input. In case of using eq. (2), the total deposited power can be expressed as:

$$P_{MW} = A \int_{z_p}^{z_p+L} Q_{MW}(z)\, dz = \frac{AL}{2} Q_{max} \qquad (3)$$

Given the lack of experimental data and the complex physics giving rise to plasma contraction (in both the axial and radial direction), it is difficult to estimate *a priori* the average power deposition density. In order to take into account the effect of pressure on the power deposition, we decided to take a maximum power deposition proportional to the pressure. The effect of power deposition will be discussed in more detail in sections 3.1, 3.2.1 and 3.3.1 below. The effect of radial contraction of the plasma is not studied here, due to the limitations of the 0D approach, which are discussed in more detail in part 3.4. Note that the triangular profile of power density is well-suited for low pressures[31]. Given the lack of analytical expressions of power density profiles at higher pressures, we have chosen to use it at all pressures investigated.

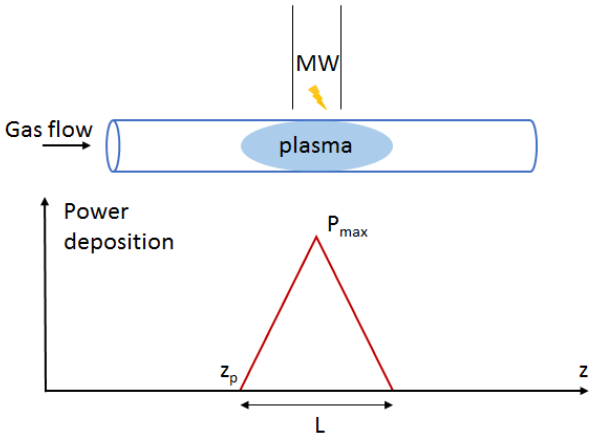

Figure 1 Simplified schematic of the surfatron MW setup modeled in this work and power deposition profile considered in the first part (3.1) of the results.

The density of the different plasma species considered in the model is obtained by solving:

$$\frac{dn_s}{dt} = \sum_j [(a_{sj}^R - a_{sj}^L)R_j] \qquad (4)$$

Where a_{sj}^R and a_{sj}^L are the right and left-hand stoichiometric coefficients of species s in reaction j, respectively, and $R_j = k_j \prod_l n_l$ is the reaction rate of reaction j. k_j is the rate coefficient of reaction j and n_l is the species density of the reactants in reaction j. Note that the surface reactions are not included in the model. At the relatively high pressures considered in this work, the characteristic time for the diffusion to the wall is typically one order of magnitude (or more) higher than the residence time. The effect of the wall is thus limited and can be neglected in this study. However, in future work, we would like to add this option to our model.

The plasma chemistry part (i.e., eq. (4)) is coupled to the Boltzmann solver Bolsig+[32] to calculate the EEDF, from which the mean electron energy and the different electron impact rate coefficients are obtained, based on cross section data.

The gas temperature T_g is either taken as an input or calculated using:

$$N\frac{\gamma k_B}{\gamma - 1}\frac{dT_g}{dt} = P_{el} - \sum_j R_j \Delta H_j - \frac{8\lambda}{R^2}(T_g - T_w) \qquad (5)$$

Where $\gamma = \frac{C_p}{C_v}$ is the specific heat ratio, k_B is the Boltzmann constant, P_{el} is the power transferred from the electrons to the heavy particles through elastic collisions, ΔH_j is the enthalpy of reaction j, λ is the gas thermal conductivity and T_w is the wall temperature, taken to be 300 K in this work. The procedure to obtain λ and γ is explained in our previous work[19,33]. The last term of the right-hand side of equation (5) corresponds to the cooling due to heat conduction[34], assuming a parabolic radial profile for the gas temperature and negligible axial gradients. Given the radial contraction of the plasma at high temperature, its behavior is in fact more complex and a 2D or 3D description of the plasma would be required to obtain a more accurate description of the gas temperature and its gradients. On the other hand, 0D modeling is sufficient, and even more appropriate for the present investigation, as it allows an accurate description of the complex chemistry taking place in the plasma and enables the assessment of the main chemical processes occurring, thus giving valuable information on how to improve the experimental CO_2 conversion.

2.2 Chemistry set

The chemistry set used is this work was developed earlier in our group.[17,19,23,24,33,35] It considers an extensive list of species presented in Table 1, which includes 25 vibrational levels of CO_2 (4 lumped symmetric mode levels + 21 asymmetric mode levels up to the dissociation limit). Furthermore, 10 vibrational levels of CO and 4 vibrational levels of O_2 are considered.

The reactions taken into account in the model are listed in the Supporting Information. This work adopts the rate coefficients of the second paper of Kozák et al.[19]. Table S1 shows the electron impact reactions, for which the rate coefficients are derived from cross section data and the EEDF. The EEDF is calculated using the cross section set proposed by Grofulovic et al.[25], which was validated from the comparison between swarm parameters calculated using a two-term Boltzmann solver and the available experimental data.

Superelastic collisions with the vibrationally excited molecules in the (0 1 0) bending mode, i.e., CO_2v_a, are included, as they might have a non-negligible effect on the EEDF[25]. The double arrows in Table S1 indicate that the reverse superelastic collisions have been included in the kinetics part of the model.
The choice of a certain electron impact dissociation cross section (here we use the Phelps cross section with threshold of 7eV, as recommended in previous studies[22,24,25,27–29]) is critical for such a study, as the difference in electron impact reaction rates can be several orders of magnitude when using different cross sections[24,36]. Note that in more recent work, Pietanza et al.[37] uses the Cosby and Helm electron impact dissociation cross section.
Table S2 lists the electron-ion recombination reactions, along with one other electron impact reaction, described by analytical rate coefficients. Table S3 shows the reactions involving ions, while Table S4 gives the neutral reactions with vibrational energy exchanges. Note that the notations for reactions involving vibrational exchanges have been changed compared to our previous work[17]. Finally, Table S5 presents the different neutral reactions included in the model.
The methods used to calculate the rate coefficients of the reactions with vibrationally excited molecules are explained in detail in Kozák et al.[17]. Note that we have not used the reduction techniques proposed in our previous work[33] in order to keep our results as accurate as possible, since we run the model in a wide range of conditions, and it is not a priori known which reactions are important or negligible at all these conditions. Moreover, the model runs fast enough to keep the full chemistry set.

Table 1: List of chemical species considered in the model

Neutral ground state species		
CO_2, CO, O_2, O, C, C_2O, O_3, C_2		
Charged species CO_2^+, CO_3^-, O^-, O_2^-, CO_4^+, CO^+, $C_2O_2^+$, $C_2O_3^+$, $C_2O_4^+$, C^+, C_2^+, O_2^+, O_4^+, O^+, CO_4^-, O_4^-, O_3^-, e^-		
Vibrationally and electronically excited states		
Name	Energy (eV)	State
$O_2v_{1\text{-}4}$	0.19, 0.38, 0.57, 0.75[26]	
$CO_2v_{1\text{-}21}$	Anharmonic oscillator [38]	(0 0 n)
CO_2v_a	0.083	(0 1 0)
CO_2v_b	0.167	(0 2 0) + (1 0 0)
CO_2v_c	0.252	(0 3 0) + (1 1 0)
CO_2v_d	0.339	(0 4 0) + (1 2 0) + (2 0 0)
$COv_{1\text{-}10}$	Anharmonic oscillator [39]	
O_2e_1	0.98[40]	$A^1\Delta$, $B^1\Sigma$
O_2e_2	8.40 eV[40]	$B^3\Sigma$ + higher triplets
CO_2*	10.5 eV[26]	$^1\Delta_u$

2.3 Post-processing of the results

Besides the species densities, the electron temperature and gas temperature, and the rates of the chemical reactions between all species, the model also calculates the CO_2 conversion and corresponding energy efficiency. The definition of CO_2 conversion is given by:

$$\chi(\%) = 100\% * \left(1 - \frac{v(z_{end}) n_{CO_2}^{total}(z_{end})}{v(z_0) n_{CO_2}^{total}(z_0)}\right) \qquad (6)$$

Where $z_0 = 0\ cm$ is the initial position and $z_{end} = 30\ cm$ is the final position. $n_{CO_2}^{total}$ is the sum of the densities of all CO_2 species included in the model. In all the cases considered here, the CO_2 density is constant at the final position ($z_{end} = 30\ cm$).

To calculate the energy efficiency, we first need to define the specific energy input (SEI):

$$SEI\left(\frac{eV}{molec}\right) = \frac{P_{MW}(W)}{\Phi(sccm)} \frac{T_{ref}(K)}{p_{ref}(Pa)} \frac{k_B}{e} \frac{60(s/min)}{10^{-6}} \qquad (7)$$

Where e is the elementary charge, used to convert J into eV, $T_{ref} = 273.15\ K$ is the reference temperature, $p_{ref} = 10^5\ Pa$ is the reference pressure. The factor 10^{-6} comes from the conversion of the flow, typically expressed in standard cm^3, into standard m^3.

The energy efficiency of the conversion is then expressed as:

$$\eta(\%) = \frac{\chi\ (\%) *\ 2.9\ (\frac{eV}{molec})}{SEI\ (\frac{eV}{molec})} \qquad (8)$$

Where $2.9(eV/molec)$ is the energy cost of splitting one CO_2 molecule into CO and 1/2 O_2.

Furthermore, the model also provides information on the relative contribution of the various vibrational levels to the dissociation mechanisms of CO_2. The relative contribution of a given level *i* is defined as:

$$X(\%) = 100\ \% \frac{\sum_{i \in j} \int_0^\tau R_i\, dt}{\sum_j \int_0^\tau R_j\, dt} \qquad (9)$$

Where the definition of τ, the integral upper bound, is explained in the text below. The index *j* refers here to all the dissociation reactions. The index *i* refers to all the reactions taking place from level v_i. In part 3.1, the contributions indicated in the text are the result of an integration from t=0 to the end of the simulation (i.e. when z=30 cm).

Finally, we also calculate the vibrational temperature of CO_2, as it provides an indication of the extent of vibrational population. The vibrational temperature is calculated from the population of the first asymmetric mode level of CO_2, since the contribution of the other levels to the total vibrational energy is typically low. It is obtained by assuming a Maxwellian distribution for the vibrational population, i.e.:

$$T_v = \frac{-E_1}{\ln(\frac{n_1}{n_0})}$$

Where E_1 is the energy of the first asymmetric mode level (0.29 eV), n_1 is its density and n_0 is the ground state density.

3. Results and discussion

3.1 Self-consistent calculation of the CO_2 conversion and energy efficiency

It is known that the gas temperature plays a very important role for energy-efficient CO_2 conversion, as will also be shown in parts 3.2 and 3.3 below. However, in practice, the gas temperature cannot easily be controlled, since it is the result of the heat produced and absorbed by the plasma. Given its importance for the conversion and in order to mimic real experimental conditions, and particularly to predict the energy efficiency for CO_2 conversion, it is necessary to include a self-consistent description of the gas temperature, as we did in our previous work[19,33]. Therefore, in this section, we perform self-consistent calculations of the plasma behavior, and we calculate the CO_2 conversion and corresponding energy efficiency as a function of pressure. The gas flow rate is kept constant in all the simulations, i.e., $\Phi = 10\ slm$. Also the SEI is kept constant, i.e., 2 eV/molec, which implies that the total power is also kept fixed. The goal of this part is to understand the different processes taking place in a realistic calculation, in order to understand what causes the limitations of the CO_2 conversion and energy efficiency. The individual effects of gas temperature, power deposition and pressure will be studied in more detail in parts 3.2 and 3.3.

Figure 2 shows the calculated CO_2 conversion and the energy efficiency as a function of pressure. The maximum power density Q_{max} is taken proportional to the pressure, ensuring that each CO_2 molecule receives the same amount of energy per time unit. We don't know the exact relationship between both, as it depends on the plasma volume, and the latter is not exactly known, so each curve corresponds to a different proportionality coefficient. For the red curve, Q_{max} = 50 W.cm^{-3} at 50 mbar and Q_{max} = 1 kW.cm^{-3} at 1 bar, while for the other curves, we used a higher power density, by multiplying the latter with a factor 2, 5 or 10, to investigate the effect of a higher power density. Since the total power input (and the SEI) are kept constant (i.e., SEI = 2 eV/molec), increasing the power density by a certain factor makes the plasma volume shrink by the same factor. Finally, the green curve shows the calculated CO_2 conversion when the cooling term (last term of equation 5) is multiplied by 10 in the afterglow (i.e. after the power deposition stops), for the normal power density profile (see detailed discussion below).

It is clear from Figure 2 that the conversion and energy efficiency are linearly proportional to each other in this case, which is logical because the SEI is kept constant, and the energy efficiency is calculated from the conversion and the SEI (see eq. 8 above). Thus, the conversion and energy efficiency show exactly the same dependency with pressure. The model predicts a maximum

conversion and energy efficiency at 400 mbar for the normal power deposition density (red curve), and at 300 mbar for the other power deposition density profiles. This trend is in agreement with previous experiments[3]. For all the cases considered here, the conversion thus increases with pressure at low pressure, reaching between 13 and 20 % conversion between 200 and 300 mbar, followed by a slow drop, reaching 6 to 7 % at atmospheric pressure. The corresponding energy efficiency is 1.45 times this value, i.e. between 19% and 30% at a pressure between 200 and 300 mbar, followed by a slow drop, reaching 11% to 15% at atmospheric pressure. These value are slightly lower than the measurements of Bongers et al.[16], where energy efficiencies of about 40 % have been found in a range between 150 and 400 mbar and for a SEI of 1.7 eV/molec. This difference may be partly explained by the complexity of the flow pattern in their setup, which makes a more detailed comparison difficult. The different approximations made in this work and their effect are discussed in part 3.4.

The effect of the power deposition density is important at low pressure and we see that a higher power deposition density increases the conversion and energy efficiency, in spite of the fact that the total power deposition, and thus the SEI, is kept constant. This indicates that at low pressure, a higher power density seems more important in determining the conversion and energy efficiency than a larger plasma volume. When the pressure increases, the difference between the different power densities becomes rather small and increasing the power deposition density even has a slightly negative impact on the conversion and energy efficiency.

We also investigated the effect of faster cooling in the afterglow, as this will affect the recombination of CO back into CO_2 (see details in part 3.2 and 3.3 below), and thus the overall CO_2 conversion and energy efficiency. It is clear from Figure 2 that, in contrast to the effect of power deposition density, the effect of a faster cooling is almost negligible at pressures below 200 mbar but it becomes particularly beneficial at pressures of 300 mbar and above. The maximum conversion and energy efficiency are then shifted between 600 and 800 mbar mbar and they reach 23% conversion, with 33% energy efficiency. At atmospheric pressure, when applying this faster cooling, the conversion reaches 20%, with 29% energy efficiency, while it was only 6% (with 10% energy efficiency) with the normal cooling term. This clearly illustrates that faster cooling in the afterglow can indeed drastically improve the CO_2 conversion and corresponding energy efficiency. The latter result is of great interest for practical applications. This faster cooling might be realized by applying a supersonic gas flow, which has indeed been demonstrated to give rise to more energy efficient CO_2 conversion[4].

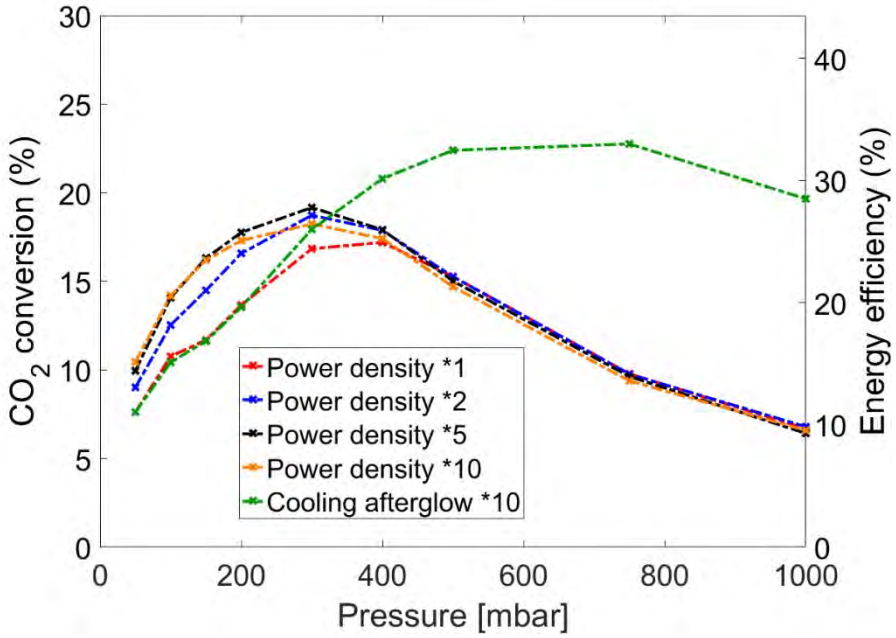

Figure 2 CO_2 conversion and corresponding energy efficiency as a function of pressure for different power deposition densities (see text) and for an increased cooling term in the afterglow (with the standard power density). Φ = 10 slm; SEI = 2 eV/molec.

To understand the trend of CO_2 conversion and energy efficiency with rising pressure, we study in detail the dissociation and recombination processes. Figure 3 illustrates the reaction rates of the three main dissociation and two main recombination mechanisms. The results are shown for three different pressures (100 mbar, 300 mbar and 1 bar) and for two different power deposition density profiles each, corresponding to the red curve of Figure 2 (i.e., Figure 3a, b, c) and to the black curve of Figure 2 (i.e., Figure 3d, e, f). The time t=0 is chosen as the beginning of the plasma, i.e., where the MW power is first applied (see Figure 1 above). The end time of the plasma is easily identifiable by looking at the electron impact dissociation rate (red curve), since this rate drops right after the plasma (i.e., when the MW power deposition drops to zero) and is negligible in the afterglow. The residence time naturally depends mostly on the size of the plasma. As the power deposition density is a factor 5 higher in the right panels (Figure 3d, e, f) than in the left panels (Figure 3a, b, c), the plasma volume is a factor 5 lower, at constant total power (and SEI). This explains why the residence time is about a factor 5 shorter in the right panels. It is not exactly a factor 5, since the gas temperature is self-consistently calculated and also plays a role in determining the residence time. Note that the time in Figure 3 can easily be transferred to the position in the plasma, by looking at Figure 1 above.

The dissociation rates are strongly correlated with the evolution of other plasma parameters, such as the electron density, the gas temperature and the vibrational temperature. Figure 4 shows the evolution of the electron density (left y-axis), as well as of the gas temperature T_g and the vibrational temperature T_v (right y-axis) as a function of time. The results are again shown for three different pressures (100 mbar, 300 mbar and 1 bar) and for two different power deposition density profiles each, i.e. the same conditions as in Figure 3 and with the normal cooling term.

In all the cases shown here, electron impact dissociation is the dominant dissociation mechanism in the first part of the plasma, i.e. before the gas temperature increases.

Further in the plasma region, i.e., at later times, the gas temperature increases due to VT relaxation and thus the rates of the neutral reactions rise. As a consequence, the two other main dissociation mechanisms (N1 and N2) become relatively more important. The gas temperature starts decreasing before the end of the plasma, since the power deposition density drops (cf. the triangular profile illustrated in Figure 1 above). At 1 bar, the gas temperature decreases more slowly, because the recombination reactions become more important (cf. Figure 3) and they are exothermic, and also because the gas has a larger heat capacity at higher pressure.

The dissociation of CO_2 upon collision with O atoms, i.e., reaction N2, is the main dissociation mechanism at the end of the plasma and in the afterglow. For high power depositions (Figure 3d, e and f), the role of reaction N1 becomes slightly more important, although at 300 mbar (Figure 3b) and 1 bar (Figure 3c), it plays a non-negligible role in the case of the lower power deposition too.

At 100 mbar (Figure 3a), electron impact dissociation is overall clearly the main dissociation mechanism. When the pressure increases, its role becomes less and less important compared to the role of reactions N1 and N2. More specifically, at 100 mbar, electron impact dissociation accounts for 66% of the entire CO_2 dissociation with both power deposition profiles. The relative contribution of electron impact dissociation clearly decreases upon increasing pressure and is only around 4% at atmospheric pressure in both cases. Reaction N1 accounts for 2%, 11% and 5% of the total dissociation at the regular power deposition profile, at 100, 300 mbar and 1 bar, respectively. Finally, reaction N2 contributes for 33 %, 59 % and 91 % to the total dissociation at 100 mbar, 300 mbar and 1 bar, respectively. On average, the relative importance of these different mechanisms is not much influenced by the choice of power deposition. However, the absolute value of the dissociation reaction rates is higher when increasing the power density, especially at low pressure. It is clear that reaction N2 is by far the most important dissociation mechanism at atmospheric pressure. However, as mentioned above, the O atoms which contribute in reaction N2 mainly originate from the reverse reaction N4, which indicates that both reactions reach a sort of equilibrium, thereby limiting the conversion at atmospheric pressure. It also explains why the cooling in the afterglow has a beneficial effect on the conversion at higher pressure. Indeed, recombination is a strong limiting factor at higher pressure and a faster cooling partly prevents these reactions from happening, as we will see below.

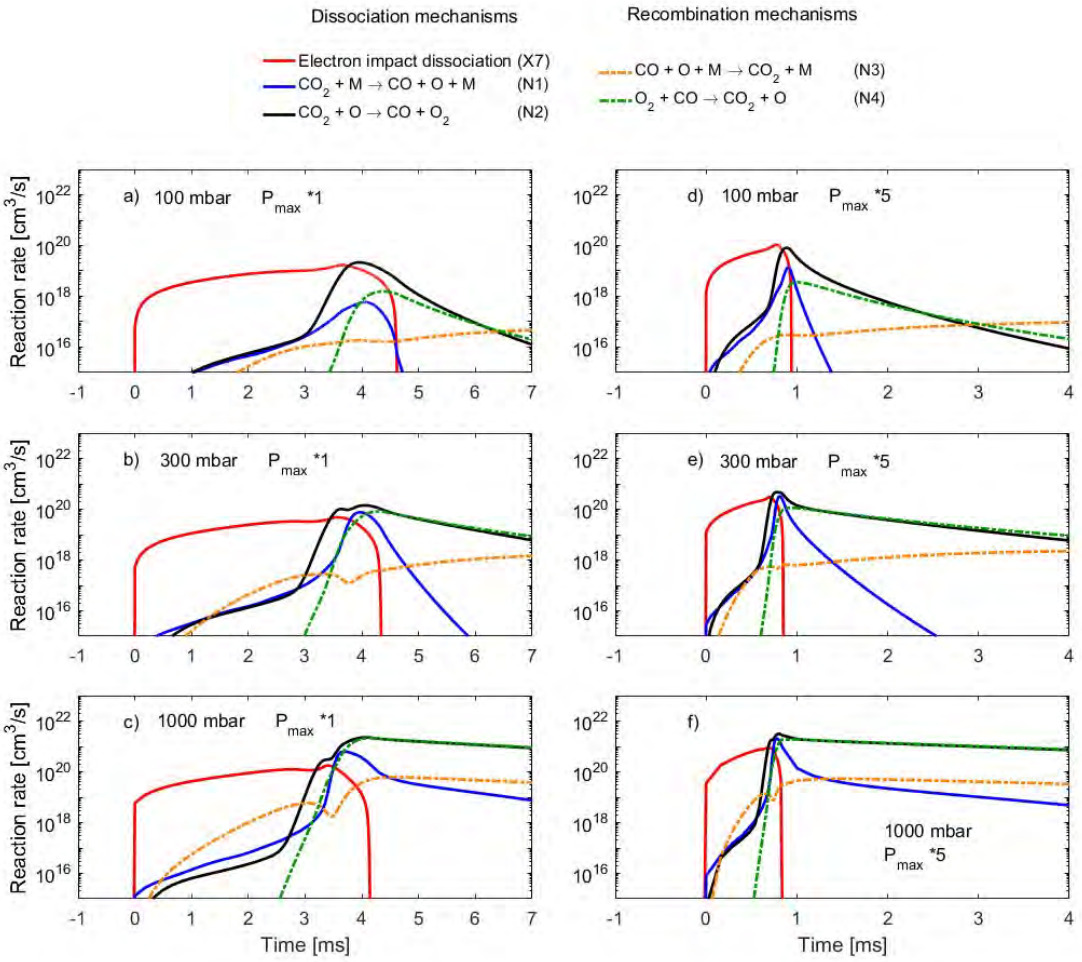

Figure 3 Reaction rates of the three main dissociation mechanisms (full lines) and two main recombination mechanisms (dashed lines), as a function of time, for three different pressures: 100 mbar (a and d), 300 mbar (b and e) and 1 bar (c and f), and for a regular power density profile (a, b and c) and a 5 times higher power profile corresponding to a plasma contracted by a factor 5 (d, e and f).

The vibrational temperature profiles, shown in Figure 4, show that the level of non-equilibrium (characterized by T_v/T_g) is higher at low gas temperatures, low pressures and high power densities. Indeed, at 100 mbar, the maximum of T_v/T_g is 2 at t=0.9 ms with the regular power deposition profile, while it reaches 3 at t=0.3 ms with the 5 times higher power deposition. At 300 mbar, the maximum T_v/T_g is 1.62 (at t=0.7 ms) and 2.2 (at t= 0.15 ms), for the normal power deposition and the 5 times higher power deposition, respectively. At 1 bar, it is 1.37 (t=0.5 ms) and 1.71 (t=0.16 ms) at the normal and 5 times higher power deposition, respectively. However, in all these cases, as soon as the gas temperature increases, the ratio T_v/T_g becomes close to 1, indicating that the vibrational distribution becomes thermal in all cases investigated. Therefore, it seems that the non-equilibrium is better exploited with low pressures and high power deposition, but even in these cases, it is only present when the gas temperature remains low. The next two parts (3.2 and 3.3) are dedicated to understand how to better exploit the non-equilibrium of the discharge and why some conditions (higher power deposition, and cooling in the afterglow) give a better conversion and energy efficiency.

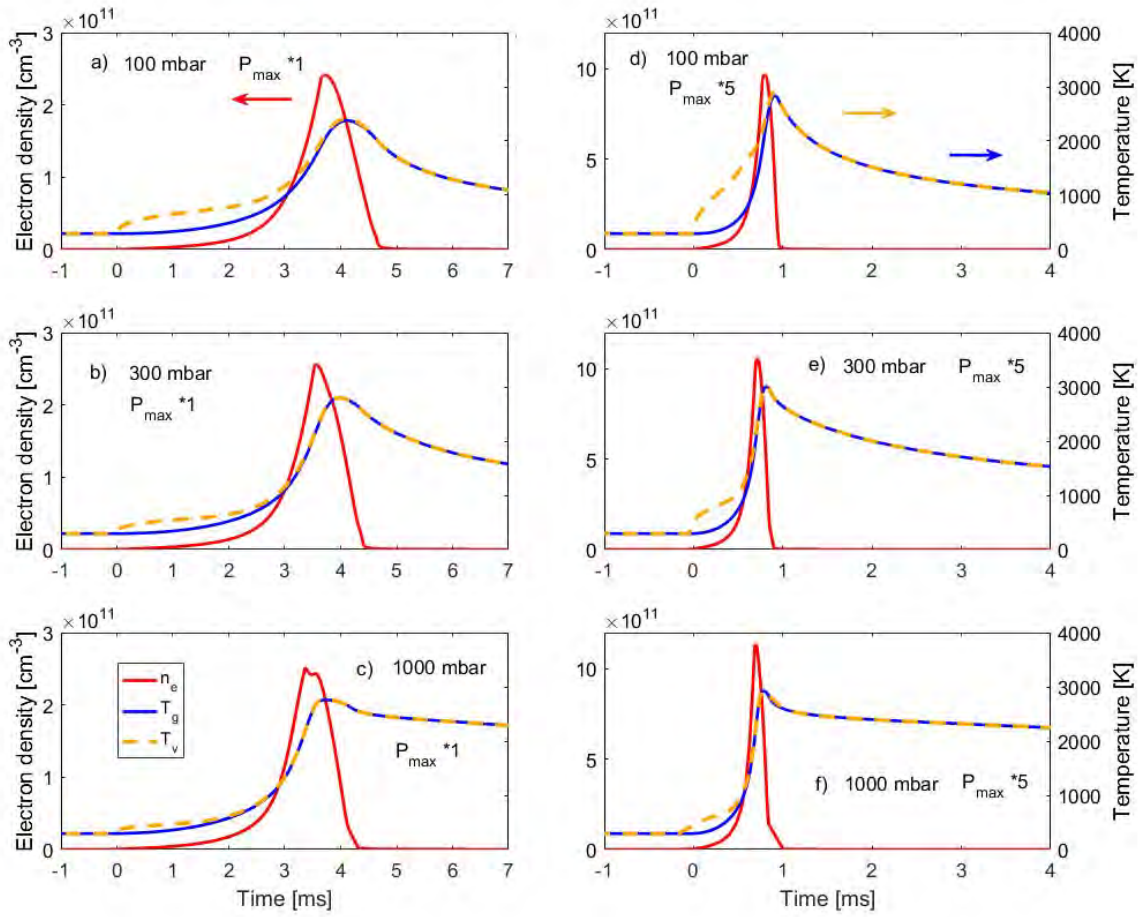

Figure 4 Evolution of the electron density n_e (red curve, left axis), the gas temperature T_g (blue curve, right axis) and the vibrational temperature T_v (orange curve, right axis), as a function of time, for three different pressures: 100 mbar (a and d), 300 mbar (b and e) and 1 bar (c and f), and for a regular power density profile (a, b and c) and a 5 times higher power profile corresponding to a plasma contracted by a factor 5 (d, e and f). Note the different y axis values for the electron density between the left and the right panels.

3.2 Vibrational distribution function (VDF)

In order to better understand the above results, we study here the effect of the different parameters (i.e., power deposition, pressure and temperature) on the vibrational distribution function (VDF). We assume here that the power deposition rises immediately from 0 to the indicated Q_{max} at t=0. The gas temperature is taken as a constant. At t=0, the gas is pure CO_2 and the VDF is taken as a Maxwellian (i.e. $n(CO_2[v_i]) = n_0 \exp(-E_i/k_bT_g)$, with n_0 a normalization constant). In this part and in part 3.3, since all the required inputs are fixed as a function of time, it is not necessary to use the plug-flow approximation. Instead, we assume that a certain power deposition Q_{max} is applied to a volume of gas V at a temperature T_g from a time t=0 to t=τ.

3.2.1 Effect of power deposition on the VDF

Figure 5 shows the VDF at a pressure of 100 mbar for two different power densities (Q_{max} = 100 W.cm^{-3} and 500 W.cm^{-3}) and two gas temperatures, i.e., 300 K (Figure 5a) and 2000 K (Figure 5b). The temperature in a MW plasma is typically between 2000 K and 3000 K[41]. However, it is generally known that a lower gas temperature can give rise to a (relatively) higher vibrational excitation and it is thus interesting to study the effect of temperature on the VDF. The VDFs are shown for different times: t=0, t=1 µs, t=10 µs and t=100 µs, which are characteristics times in the temporal evolution of the plasma (see below). In most cases, a quasi-equilibrium is reached at t=100 µs (or before). The VDF at t=0 is assumed to be Maxwellian (straight line on the y-log plot) with vibrational temperature being equal to the gas temperature. When applying microwave power, the vibrational level population gradually increases. The higher the power deposition density, the faster the increase of the vibrational population. The vibrational excitation eventually saturates, to a level that depends on the conditions.

At a gas temperature of 300 K, for both power deposition values, a quasi-steady state is reached at around 100 µs (orange curves). In case of a power deposition of 100 W.cm^{-3}, the vibrational temperature reaches 1050 K at t=100 µs, while in case of a power deposition of 500 W.cm^{-3}, the vibrational excitation is much more pronounced and the vibrational temperature reaches 2120 K. Note that these values are much higher than the gas temperature of 300 K, clearly demonstrating the non-equilibrium character of the MW plasma at these conditions. The intermediate vibrational levels from v_5 to v_{15} more or less form a plateau and thus have very similar populations. This is due to the effectiveness of energy exchange between two vibrational levels (i.e., so-called VV relaxation), as described in Treanor *et al.*[18]. For levels with higher energies (i.e., above v_{15}), the dissociation rate coefficients are much higher (due to a lower activation energy). Therefore, the population of these levels is lower since their lifetime is much shorter. This phenomenon is described in more detail in part 3.2.3 below. The difference in vibrational excitation with power deposition can easily be explained: the higher the power deposition, the higher the electron density, since more energy is available to ionize the CO_2 molecules. Indeed, at t=100 µs, the electron density is calculated to be 2.3x10^{16} m^{-3} and 1.2x10^{17} m^{-3} for a power deposition of 100 W.cm^{-3} and 500 W.cm^{-3}, respectively. It is interesting to note that the electron density is almost proportional to the power deposition for a given pressure and gas temperature. The electron temperature stays, however, practically the same at around 1.8 eV. Indeed, the higher power density gives rise to a higher electron density, so the applied energy has to be distributed over more electrons, explaining why their mean energy does not rise with higher power density. Note that the values of electron density that are self-consistently calculated here are lower than the ones used in our previous work[19]. Indeed, in Kozák et al[19], relatively high values, above the range that would be expected for typical MW plasma conditions, were used as a way to show how to optimize vibrational excitation for a given pressure and E/N, but they were not self-consistently calculated in the model.

At 2000K, the population of the vibrational levels in a Maxwellian distribution, i.e., at t=0, is of course much higher, because more energy is available for populating these levels thermally. Therefore, the effect of the plasma on the VDF is less obvious, although some overpopulation for levels v_5 and higher is still clearly visible. Furthermore, a quasi-equilibrium is reached faster (i.e., within less than 1 µs; see Figure 5b) for both power deposition values. Because the energy exchange upon collision between vibrational levels and ground state molecules, which depopulates the vibrational levels, i.e., so-called VT relaxation, increases with gas temperature, the VDF tends to become more thermalized at higher

gas temperature. Starting from t=1 µs, the vibrational temperature is calculated to be 2060 K and 2290 K for a power deposition of 100 W.cm^{-3} and 500 W.cm^{-3}, respectively. These values are only slightly higher than the gas temperature, indicating that the MW plasma tends to be close to thermal equilibrium at these conditions.

In summary, we can state that a higher power deposition gives rise to more vibrational excitation, whereas a higher gas temperature tends to thermalize the VDF. This is consistent with our previous findings (Figure 4), where we saw that the value T_v/T_g is higher in those regions of the discharge characterized by a low gas temperature is low and a high power deposition.

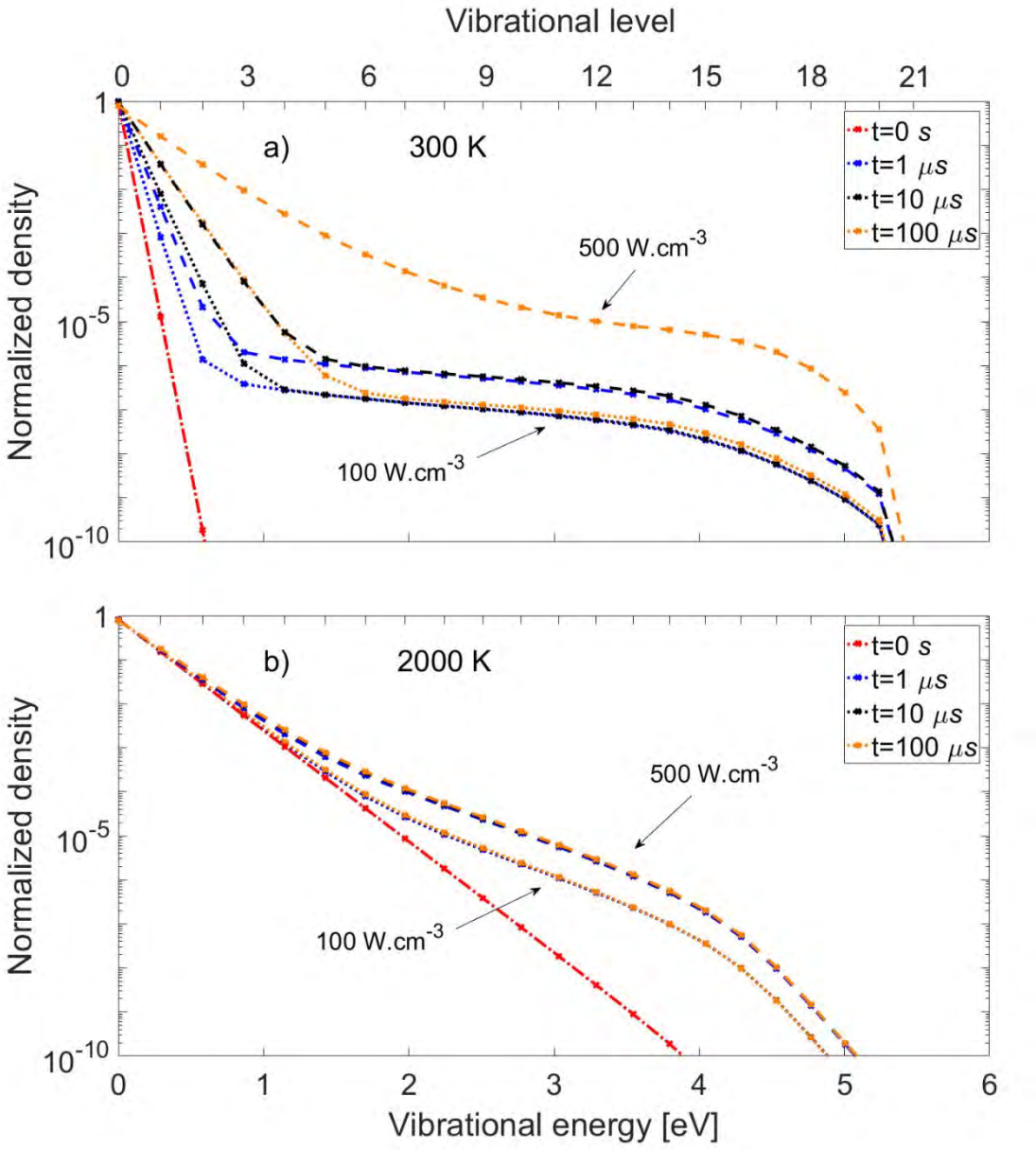

Figure 5 Vibrational distribution functions at different times (see legend) for a gas temperature of 300 K (a) and 2000 K (b) and a pressure of 100 mbar. The results are shown for two different power densities: Q_{max} = 100 W.cm^{-3} (dotted lines) and Q_{max} = 500 W.cm^{-3} (dashed lines).

3.2.2 Effect of pressure on the VDF

Figure 6 shows the VDF at different times (t=0, t=1 µs, t=10 µs and t=100 µs), again for a gas temperature of 300 K (Figure 6a) and 2000 K (Figure 6b). Two different pressures and corresponding power densities are considered, i.e., 50 mbar at 50 $W.cm^{-3}$ and 1 bar at 1 $kW.cm^{-3}$. Note that we again assume the power deposition to be proportional to the pressure, ensuring that each CO_2 molecule receives the same amount of energy per time unit, so that we can better evaluate the effect of pressure.

At a gas temperature of 300 K and atmospheric pressure (1 bar), the VDF reaches a quasi-steady state after 10 µs. The vibrational temperature reaches 620 K, despite the high power deposition. At lower pressure (50 mbar), a quasi-steady state is reached only after approximately 100 µs. The shape of the VDF is similar to the VDF in the 1 bar case. However, the vibrational temperature reaches 1170 K, indicating that the MW plasma is more out-of-equilibrium at lower pressure. For comparison, at 100 mbar and 100 $W.cm^{-3}$, the vibrational temperature was calculated to be 1050 K (see previous section), hence in between the results at 50 mbar and 1 bar, clearly illustrating the effect of the pressure. At 50 mbar, the plateau is also present but with a population about 1 order of magnitude higher than at atmospheric pressure. This is mainly due to the higher VT vibrational energy losses in the plasma at atmospheric pressure, resulting in a less pronounced degree of vibrational excitation.

At a gas temperature of 2000 K, the VDF reaches again a quasi-steady state much faster, in less than 1 µs. The difference with a Maxwellian distribution is only significant from level v_5 at 50 mbar and from level v_8 at 1 bar. The overpopulation from the Maxwellian distribution, or in other words, the degree of non-equilibrium, is again obviously less important compared to the 300 K case. However, the normalized density of the vibrationally excited levels is higher at 2000 K than at 300 K, both at 50 mbar and at 1 bar, because the levels are also partially thermally populated.

Thus, we can conclude that a higher pressure, just like a higher temperature, tends to make the VDF thermalize faster and it is thus detrimental for the vibrational excitation. This is also consistent with our previous results (Figure 4), which revealed that the ratio T_v/T_g was maximum at low pressures and low gas temperatures.

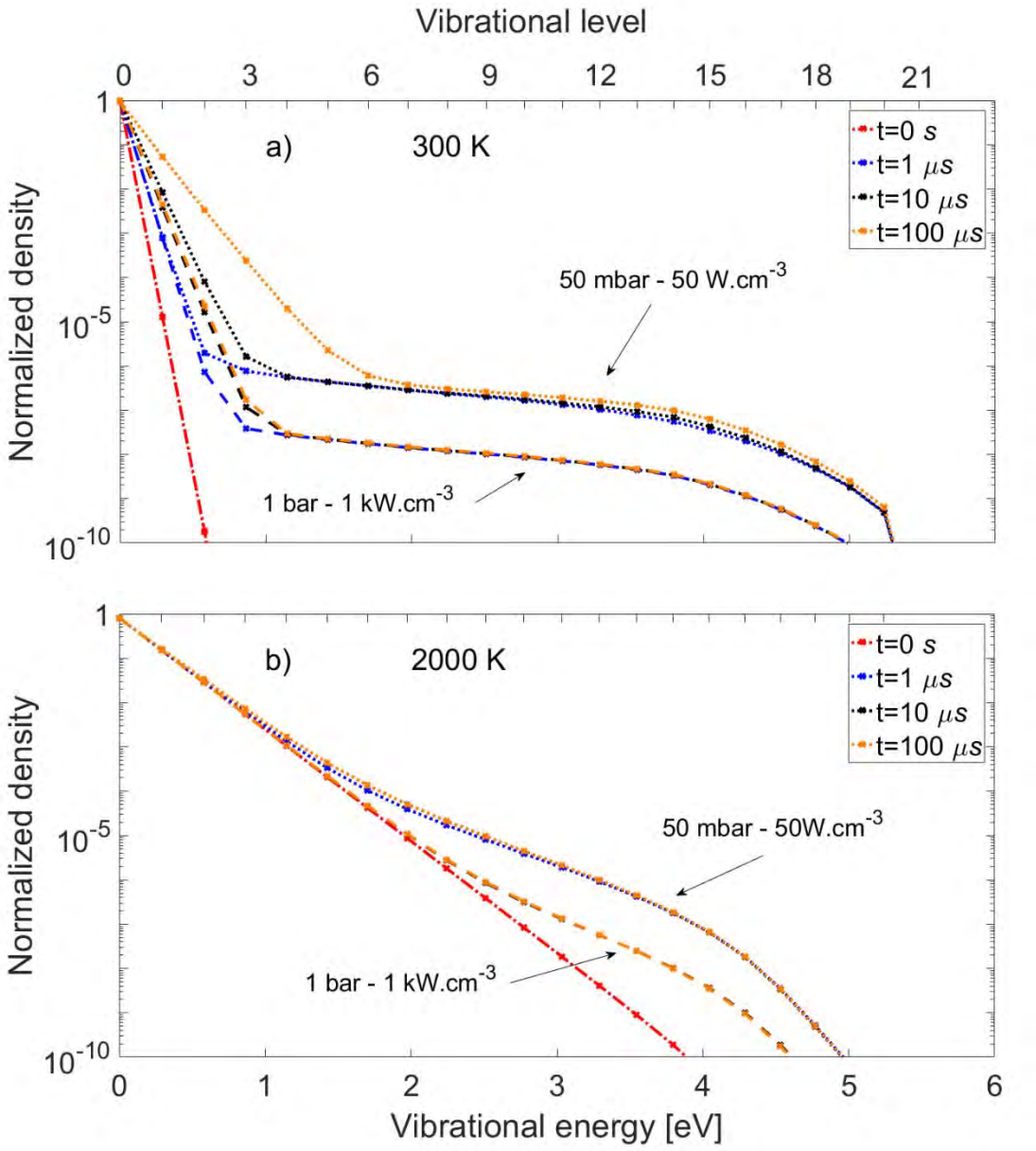

Figure 6 Vibrational distribution functions at different times (see legend) for a gas temperature of 300K (a) and 2000K (b). The results are shown for two different pressures and power densities: p=50 mbar and Q_{max}= 50 W.cm^{-3} (dotted lines) and p=1 bar and Q_{max}=1 kW.cm^{-3} (dashed lines).

3.2.3 Effect of dissociation and vibrational-translational (VT) relaxation reactions on the VDF

It is known that the Treanor distribution has a higher population of the highest vibrational levels, and this would be beneficial for CO_2 splitting, because these levels tend to dissociate easily. However, the VDFs shown above do not exhibit this Treanor distribution. The reason is that the classical Treanor distribution is derived for the case of anharmonic molecules without dissociation reactions and VT relaxation. To demonstrate this, we show here the effect of the dissociation reactions and VT relaxation on the VDF. For this purpose, we considered a chemistry set without dissociation reactions

(i.e. the reactions N1, N2, N5, X3, X4, X5, X6 and X7 from Table S1 and Table S5 in the Supporting Information are removed, as well as all the reactions from Table S3 involving the CO_2 molecules) and a set without dissociation reactions and VT relaxation (reactions V1, V2a, V2b and V2c from Table S4). We compare the results with those obtained using the full chemistry set. Figure 7 shows the VDF obtained using the full chemistry set and the chemistry set without dissociation reactions at t=300 µs, for a gas temperature of 300 K, a pressure of 50 mbar and a power deposition density of 200 $W.cm^{-3}$. At this time of 300 µs, a quasi-equilibrium has been reached for the VDF. Note that this quasi-equilibrium is reached after a longer time in the case without dissociation. We also compare with the corresponding Maxwellian distribution at a temperature of 300 K and with the Treanor distribution at a gas temperature of 300 K and a vibrational temperature of 3010 K. The latter corresponds to the vibrational temperature of the actual VDF calculated without dissociation reactions (see below). Note that a relatively high power density, a low pressure and a low gas temperature are used for this comparison, in order to clearly show the Treanor effect. Indeed, with a lower power density and a higher gas temperature and pressure, as shown above, the vibrational excitation is weaker, and both the actual VDF and the Treanor distribution are then closer to a Maxwellian distribution. It is thus more difficult to observe the Treanor effect.

The comparison between the two VDFs obtained with and without dissociation reactions shows that without dissociation, the highly excited levels are more populated than when dissociation is considered. This is very logical, and attributed to the large dissociation rate coefficients associated with these levels, since the activation energy of the different dissociation reactions is significantly lower for the highly excited levels. It is interesting to note that when neglecting dissociation, the highest levels of the VDF are even more populated than the intermediate levels, as is also the case for the Treanor distribution. The vibrational temperature is calculated to be 2500 K with dissociation and 3010 K without dissociation reactions.

The VDF calculated without dissociation reactions is in reasonable agreement with the analytical predictions of Treanor et al.[18], in which the dissociation reactions were also not considered. A large difference is still visible for the highly-excited levels, as the Treanor distribution predicts a higher population of these levels. However, in reality, dissociation of CO_2 does take place, and thus, it is clear from Figure 7 that the Treanor distribution greatly overestimates the real VDF, and can thus not be used to predict CO_2 splitting in a plasma in a realistic way.

Finally, the VDF calculated without dissociation and VT relaxation reactions (green curve in Figure 7) has a similar shape as the one without dissociation (black curve in Figure 7) but its vibrational temperature is much higher (i.e., 4300 K compared to 3010 K), clearly demonstrating that VT relaxation is also responsible for the loss of vibrational energy.

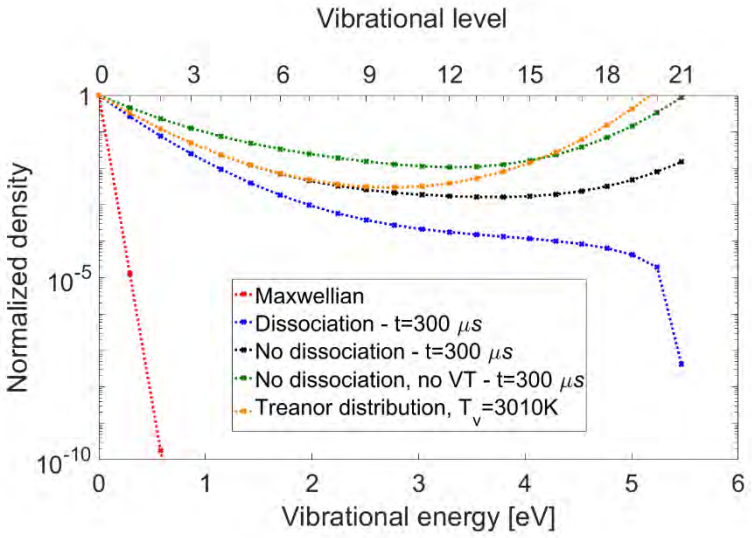

Figure 7 Vibrational distribution functions at a pressure of 50 mbar, a power density of 200 W.cm^{-3} and a gas temperature of 300 K. The blue curve corresponds to the VDF obtained using the full chemistry set. The black curve was obtained by neglecting the dissociation reactions. The green curve was obtained by neglecting the dissociation reactions and the VT relaxation reactions. The orange curve is calculated using the analytical formula of a Treanor distribution, while the red curve shows a Maxwell distribution at 300 K.

3.3 Dissociation and recombination mechanisms of CO_2

Now that we understand how the VDF varies with the operating conditions, we want to investigate the effect on the dissociation and recombination mechanisms of CO_2, to better understand the self-consistently calculated CO_2 conversion and energy efficiency in the range of conditions investigated in part 3.1. The same conditions as in the previous part (3.2) are considered here: the VDF is Maxwellian at t=0 and the power deposition rises from 0 to Q_{max} at t=0. In all the conditions tested here, our calculations predict that the main dissociation mechanisms of CO_2 are electron impact dissociation, and dissociation upon collision with O atoms or any other molecule (denoted as M), i.e., reaction X7 ($CO_2 + e^- \rightarrow CO + O + e^-$) in Table S1, and reactions N1 ($CO_2 + M \rightarrow CO + O + M$) and N2 ($CO_2 + O \rightarrow CO + O_2$) in Table S5 from the Supporting Information. The reaction rates shown here are taken as the sum of the reaction rates from the ground state and vibrationally excited states.

To compare the data, we introduce the quantity τ, which is the time after which each molecule in the considered volume has received an energy of 1eV in average:

$$\tau = \frac{p}{T_g Q_{max}} \frac{e}{k_B}$$

Where e is the elementary charge, used to convert J into eV, p is the pressure and Q_{max} is the power deposition density, both expressed in SI units. This allows us indeed to compare the average reaction rates in a period during which each CO_2 molecule has received the same amount of energy, so that the latter is kept constant. τ can thus be considered as a characteristic time of the plasma, which would be the residence time in a discharge with a SEI of 1 eV/molec. The rates are thus averaged in the plasma only, and not in the afterglow, although the variations of the rates in the afterglow with the gas

temperature can be inferred from these results. This averaging is necessary to compare the different data. However, since the time τ varies with the conditions, this averaging can have some consequences on the results, which are indicated in the text.

3.3.1 Effect of power deposition on the dissociation and recombination mechanisms

Figure 8 shows the reaction rates of the three main dissociation processes of CO_2, as well as the two main recombination processes, forming again CO_2, for different values of power deposition and gas temperature, at a pressure of 100 mbar. The reaction rates are averaged from t = 0 to t = τ. Note that the density of the gas molecules changes with the gas temperature (according to the ideal gas law), thus the absolute value of the reaction rates also changes, since it depends on the density of the reactants.

At T_g = 300 K (Figure 8a), electron impact dissociation is the main dissociation process for low power deposition: from 50 to 200 W.cm^{-3}, reactions N1 and N2 are negligible. However, when the power density increases, these two reactions become increasingly important and end up contributing even slightly more than electron impact dissociation. At T_g=1000 K (Figure 8b) and T_g=2000 K (Figure 8c), electron impact dissociation is by far the main dissociation mechanism, while reactions N1 and N2 are almost negligible. Finally, at T_g=3000 K (Figure 8d), electron impact dissociation is not so important at low power deposition (i.e., below 200 W.cm^{-3}), but it becomes increasingly important upon higher power deposition, while the importance of N1 and N2 stays almost constant with increasing power deposition.

Note that in all the cases shown here, the average value of the electron impact dissociation rate linearly increases with power deposition. This can be explained by the fact that the electron density also linearly increases with power deposition, while the electron temperature stays constant and thus the rate coefficient stays almost constant.

At all the conditions shown here, the two major recombination reactions forming again CO_2, i.e., the three-body recombination of CO with O atoms (reaction N3 from Table S5) and the two-body recombination of CO with O_2 molecules (reaction N4 from Table S5), are almost negligible compared to the dissociation reactions at this low pressure of 100 mbar. This means that no equilibrium has been reached yet between the dissociation reactions and their reverse recombination processes. Only at T_g = 3000 K, reaction N4 has a reaction rate comparable to electron impact dissociation for low power deposition values. However, the average rate of this recombination process clearly decreases with increasing power deposition. This is caused by the fact that τ drops upon rising power deposition. Therefore, the rate is averaged over a shorter time, at the beginning of the conversion. During this time τ, the reaction products of CO_2 splitting (CO and O_2) do not have time to build up yet. Indeed, since most of the conversion is thermal in this case, the rise in CO_2 dissociation with power deposition is not important enough to counter-balance the decrease of the averaging time τ.

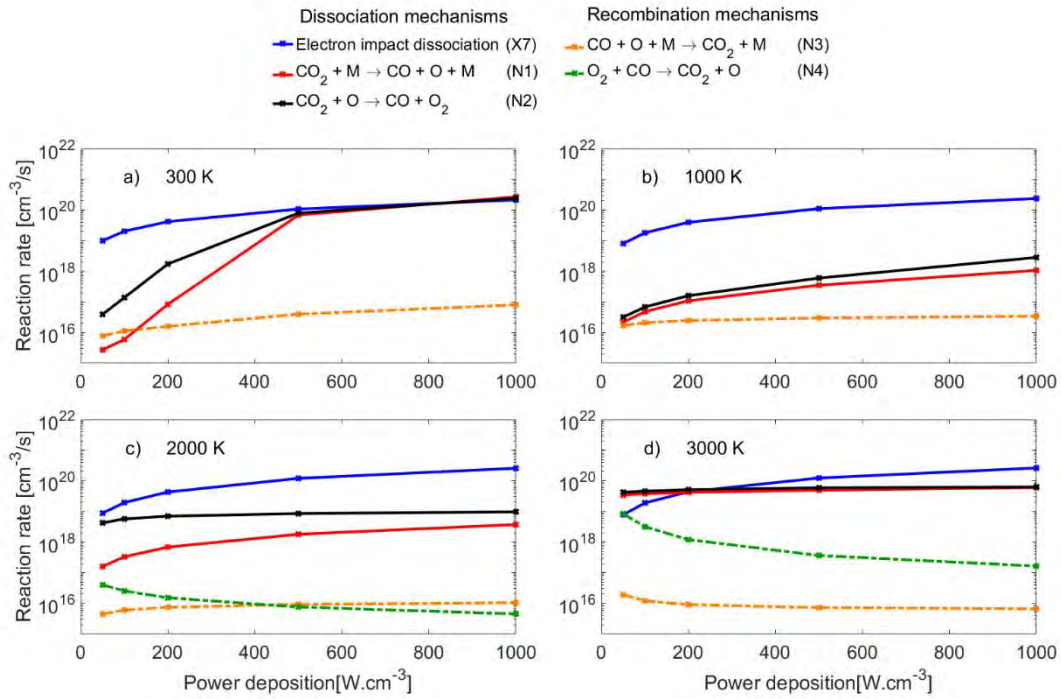

Figure 8 Reaction rates of the three main dissociation mechanisms of CO_2 (X7, N1, N2; solid lines) and the two main recombination mechanisms forming again CO_2 (N3, N4; dashed lines), averaged from t=0 to t=τ, as a function of the power deposition, for a pressure of 100 mbar, and a gas temperature of 300 K (a), 1000 K (b), 2000 K (c) and 3000 K (d).

To understand the behavior of the dissociation reaction rates of X7, N1 and N2 as a function of power deposition and gas temperature, it is interesting to look at the effect of vibrational excitation on the overall dissociation. Indeed, since the dissociation reactions have much larger probabilities to occur from a highly excited vibrational state, the total rate of a given dissociation reaction also depends on the vibrational excitation. Figure 9 shows the relative contributions of all the vibrational levels to the overall dissociation at a pressure of 100 mbar. The contributions are again averaged from t = 0 to t = τ.

At a gas temperature of 300 K (Figure 9a), the highly excited vibrational levels of the asymmetric mode are not important for dissociation at low power deposition, but they become increasingly important for high power deposition, as could also be deduced from Figure 5a above. This explains why the dissociation reactions upon impact by O atoms or any molecules M (i.e., reactions N1 and N2) become increasingly important at higher power deposition, because at low gas temperatures these reactions only occur for the highly excited vibrational levels, due to their high threshold energies. The shape of the curves in Figure 9a can easily be understood by looking at Figure 5a: the activation energy of these dissociation reactions decreases with rising vibrational energy and thus the corresponding rate coefficient increases exponentially. The plateau described previously in the VDF, with practically constant populations of the vibrational levels, then gives rises to a large contribution of the highly-excited levels. This plateau is responsible for the sudden increase of the contribution of the excited levels around level v_8. On the other hand, the intermediate levels do not have a large enough population to contribute significantly to dissociation, given the high activation energies of the reactions taking place from these levels.

At a gas temperature of 1000 K and 2000 K (Figure 9b and Figure 9c), the model predicts a quasi-negligible role of the vibrational levels with energies above 1 eV (i.e., level v_4 and higher). The dissociation almost exclusively originates from the first levels of the VDF, due to electron impact (see Figure 8b,c), and the contribution of vibrational excitation to the dissociation is not important.

Finally, at 3000 K (Figure 9d), the lowest levels are still more important, but almost all the levels, except for the highest ones, have a significant contribution to the total dissociation. This is mainly because these levels are thermally populated at this high gas temperature.

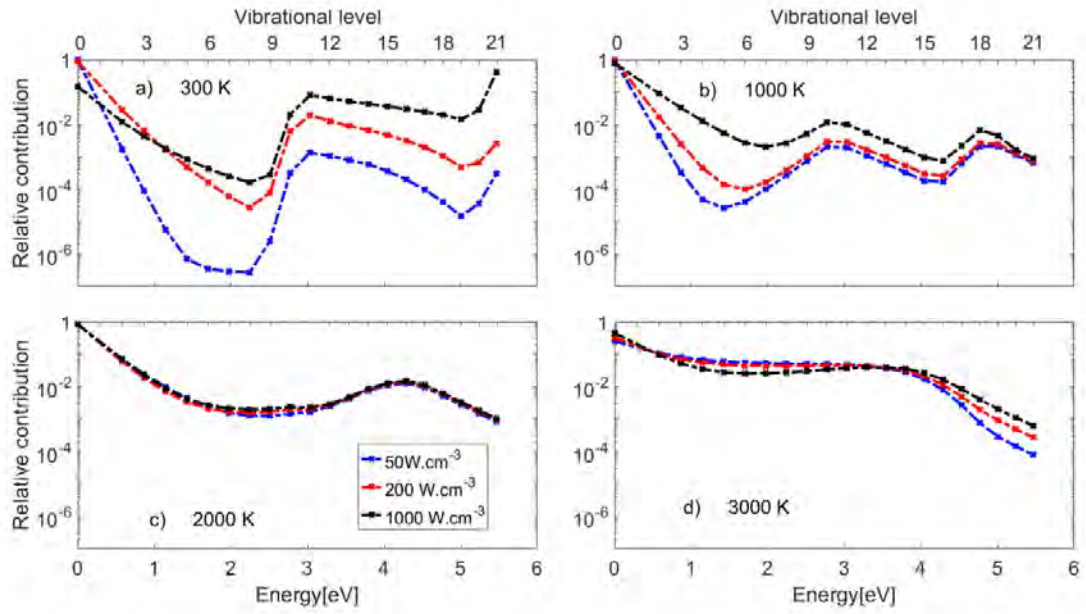

Figure 9 Relative contribution of the vibrational levels to the overall CO_2 dissociation at a pressure of 100 mbar, for different values of power density (see legend) and different gas temperatures, i.e., 300 K (a), 1000 K (b), 2000 K (c) and 3000 K (d).

As shown in Figure 5a, at T_g = 300 K, the plasma significantly affects the VDF, especially for high power deposition densities. Therefore, despite the low gas temperature and the high activation energies of reactions N1 and N2, as well as the high energy threshold for X7, vibrational excitation can become high enough to significantly enhance the probability of reactions N1 and N2 (and X7) to occur. Indeed, the energy of the highly-excited vibrational levels is comparable to the activation energy of reaction N1 (5.6 eV) and even higher than the activation energy of reaction N2 (1.43 eV). The limiting factor for reaction N2 to occur is thus mainly the presence of O atoms.

On the other hand, at higher gas temperatures, the contribution of the plasma to the vibrational excitation gradually drops, as was clear from Figure 5b above. At 1000 K and 2000 K, the gas temperature is not yet high enough to overcome the activation energy of reactions N1 and N2. Yet, at these higher gas temperatures, the VT vibrational energy losses are larger, reducing the role of the vibrational levels. This makes electron impact dissociation by far the main source of dissociation. Given the relatively low population of the highly excited vibrational levels at these temperatures, electron impact dissociation is much more likely to happen from the CO_2 ground state.

At 3000 K, the VDF does not depend much on the plasma either. However, due to the high gas temperature, the vibrational levels are more populated even at close-to-equilibrium conditions, and

the probability of reactions N1 and N2 becomes more important, both from the ground state and from vibrationally excited states. Therefore, the contribution of almost all the levels to the CO_2 dissociation becomes significant.

This explains why the reaction rates of reactions N1 and N2 do not depend much on the power deposition density at high gas temperatures, since the VDF is not so much influenced by the plasma.

In summary, at low gas temperature, electron impact dissociation, mainly from the CO_2 ground state, is the major dissociation mechanism at low power density, but at higher power densities, the dissociation reactions upon impact of O atoms or other molecules with the highly excited vibrational levels of CO_2 become increasingly important. Upon increasing gas temperature, i.e., 1000 and 2000 K, electron impact dissociation, mainly from the CO_2 ground state, is most important at all power densities, because the CO_2 vibrational levels are not enough populated, and consequently, the heavy particle reactions (N1 and N2) are not important. Finally, at a gas temperature of 3000 K, dissociation upon impact of O atoms or any other molecules (N1, N2) with the excited vibrational levels is comparable to electron impact dissociation, but in this case, the VDF is nearly thermal, so we do not really exploit the non-equilibrium conditions of the plasma. Therefore, in order to exploit the non-equilibrium aspect of the plasma, it is better to design a setup that would limit the gas temperature increase, while giving a strong power density that would enable a large vibrational excitation. This corresponds to our previous observations (Figure 3 and Figure 4), where we saw that the non-equilibrium was favored at low gas temperatures and high power deposition.

3.3.2 Effect of pressure on the dissociation and recombination mechanisms

Figure 10 shows the reaction rates of the three main dissociation processes and the two main recombination processes for different values of pressure and gas temperature. The power density again proportionally increases with pressure such that each CO_2 molecule receives the same amount of energy per time. More specifically, the power density is 50 $W.cm^{-3}$ at 50 mbar, and rises to 1 $kW.cm^{-3}$ at 1 bar. Note that these power densities correspond to the low range of power densities used above, where the pressure was kept constant at 100 mbar (so the corresponding power density is then 100 $W.cm^{-3}$; hence in the lower range of power density values of Figure 8 above). The reaction rates are again averaged from t = 0 and t = τ.

At T_g = 300 K (Figure 10a) and T_g = 1000 K (Figure 10b), electron impact dissociation is the main dissociation mechanism, by several orders of magnitude, and the heavy particle reactions (N1, N2) are not important in the entire pressure range, which is attributed to the relatively low values of the power density used here (cf. Figure 8 above). Indeed, at low power density, vibrational excitation is limited, and the heavy particle reactions (N1, N2), which mainly occur with the vibrational levels, are thus not important. At higher power densities, these reactions become gradually more important, as was obvious from Figure 8. At T_g = 2000 K (Figure 10c), reaction N2 becomes more and more important and is of the same order of magnitude as electron impact dissociation. At T_g = 3000 K (Figure 10d), electron impact dissociation becomes of lower importance, especially with increasing pressure, while reaction N2 has the largest reaction rate.

The recombination reactions have increasing reaction rates with increasing pressure. However, from T_g = 300 K to T_g = 2000 K, their rates are clearly lower than the total dissociation rate. On the other

hand, at T_g = 3000 K (Figure 10d) and for high pressures (above 500 mbar), the recombination reaction N4 plays a significant role and has a rate larger than N1, and comparable to N2. The O atoms consumed by reaction N2 actually originate from the recombination of O_2 and CO. This suggests that an equilibrium has been reached between the dissociation reaction (N2) and the recombination reaction (N4), limiting the CO_2 conversion at high temperature and atmospheric pressure

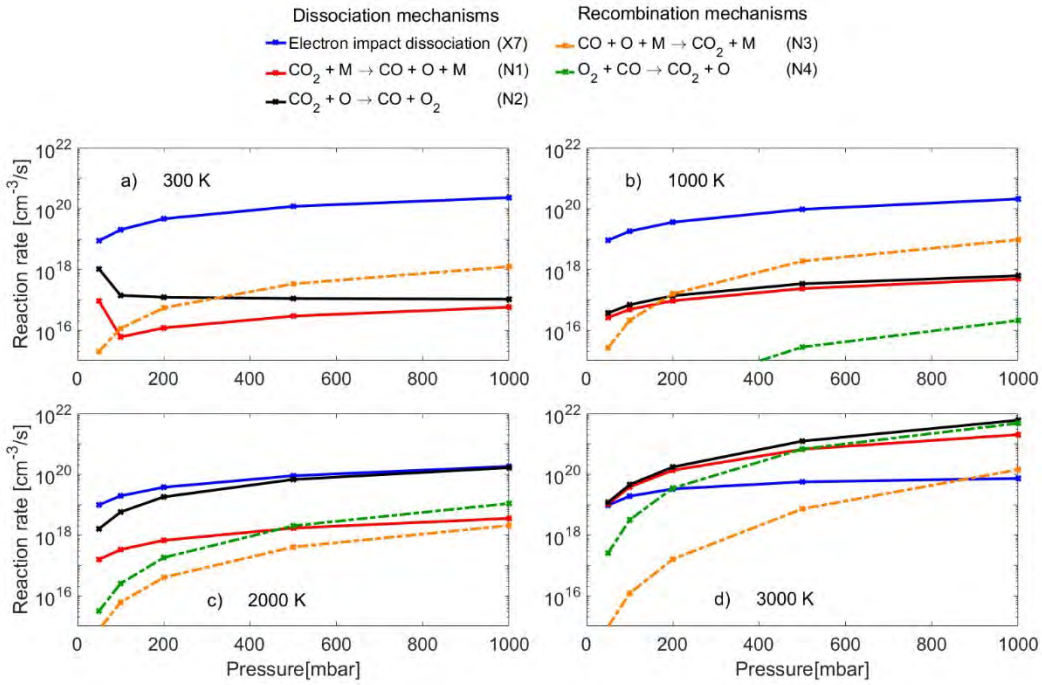

Figure 10 Reaction rates of the three main dissociation mechanisms and two main recombination mechanisms, averaged from t=0 to t=τ, as a function of pressure. The power deposition density increases linearly with pressure. Each panel corresponds to a different gas temperature: 300 K (a), 1000 K (b), 2000 K (c) and 3000 K (d).

Figure 11 shows the relative contributions of the vibrational levels to the dissociation reactions (X7, N1 and N2) at three different pressures and four different temperature values. The contributions are again averaged from t = 0 to t = τ. At T_g = 300 K (Figure 11 a), most of the dissociation takes place from the ground state. However, the highly-excited states also play a non-negligible role, as in Figure 9, especially at 50 mbar. At T_g = 1000 K (Figure 11 b) and T_g = 2000 K (Figure 11 c), the contribution of the highly excited levels is not very important to the total dissociation, as also seen before in Figure 9. At T_g = 3000 K (Figure 11 d), the contribution of all the vibrational levels is more important, except for those with the highest energies. As explained before, this is due to the fact that the conversion is mainly caused by thermal processes rather than by plasma processes.

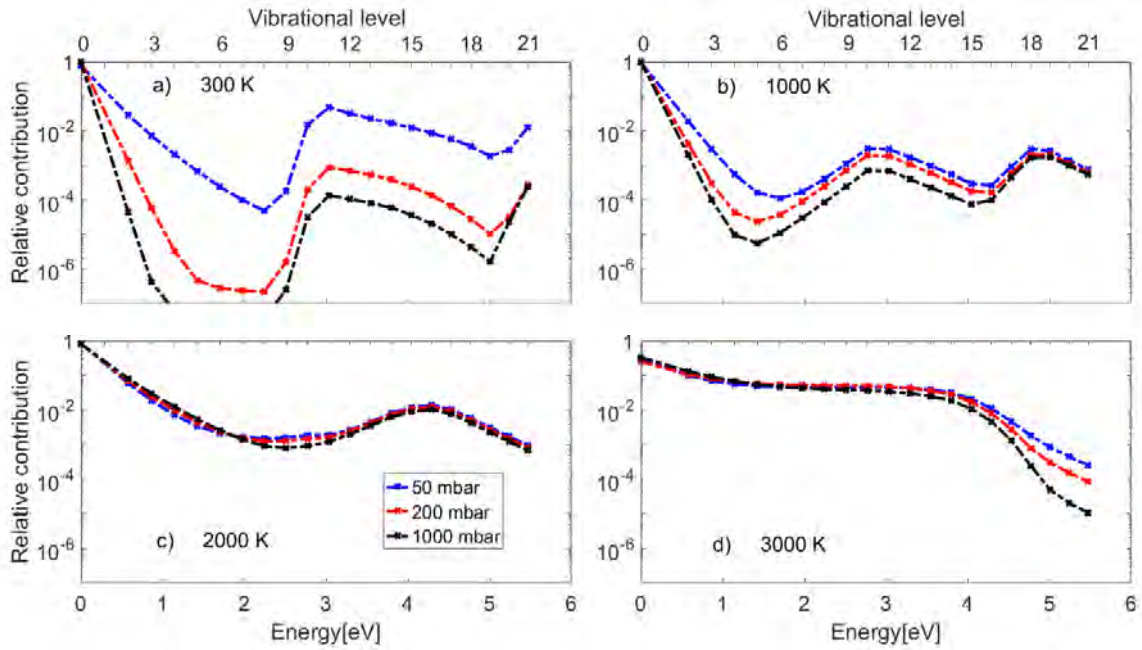

Figure 11 Relative contribution of the vibrational levels to the overall dissociation for different values of pressure (see legend) and different gas temperatures, i.e., 300 K (a), 1000 K (b), 2000 K (c) and 3000 K (d).

For all the cases shown here, the role of vibrational excitation is more important at lower pressure than at atmospheric pressure. This can be understood again by looking at Figure 6, which shows that upon increasing pressure the VT relaxation rises, and tends to thermalize the VDF. On the other hand, as seen in Figure 10d, a higher pressure favors the heavy particle dissociation reactions more than electron impact dissociation for high gas temperatures. We can thus conclude that a lower pressure tends to make the plasma more non-equilibrium and improves the role of vibrational excitation. Furthermore, the role of recombination reactions is also reduced at lower pressures. Both effects are beneficial for the CO_2 conversion.

These results explain the dependence of the conversion to the different parameters observed in Figure 2. Indeed, as seen from Figure 3, Figure 4 and Figure 10, at low pressure, despite the larger vibrational excitation, electron impact dissociation is the main dissociation process, which is not very efficient, and the heavy particle reactions N1 and N2 only account for a small fraction of the total dissociation. The role of these two reactions increases with pressure, especially at relatively high gas temperatures. On the other hand, an increase in pressure has two detrimental effects on the conversion: (i) the vibrational distribution thermalizes faster and (ii) recombination reactions become more important. Hence, the CO formed in the discharge recombines in the afterglow due to the large recombination reaction rates and the slower drop in gas temperature. This explains why increasing the cooling in the afterglow has a beneficial effect on the conversion at high pressure (see green curve in Figure 2): (i) at low pressure, recombination is not so important and a faster cooling is thus not particularly beneficial, while (ii) at high pressure, a large fraction of the CO formed in the discharge recombines in the afterglow, which can be partly prevented with a better cooling.

Our results also indicate that a higher power density yields more pronounced vibrational excitation (see Figure 5) and gives a stronger weight to the heavy particle reactions (N1 and N2) in the dissociation process, especially at low gas temperatures.

3.4. Limiting factors and how to take optimal advantage of the non-equilibrium in a MW discharge

The above results are very interesting, but we would like to point out the limitations of the model in order to better understand these results and how they compare to experiments. First, the approximations required by the 0D approach are not necessarily valid in all cases. In reality, the power deposition and the gas temperature also depend on the radial coordinate and the complexity of these gradients cannot be reproduced here. Moreover, at high pressures, the plasma also tends to contract in the radial direction, resulting in a layer of gas around the plasma, which has a large influence on the gas temperature gradients. This contraction makes the plasma smaller and therefore it increases the power density. According to experimental data[41], increasing the pressure causes a sharp transition from diffuse to contracted regimes. These effects are obviously not captured by our 0D approach.

Furthermore, the chemistry set also contains some approximations. The rate coefficients are not always well known, which might hinder the accuracy of the results. Our modeling work would benefit greatly from more in-situ experimental measurements (electron density, gas temperature, …) in order to benchmark our results. It should also be pointed out that the effect of the CO_2 vibrational levels of the symmetric mode at high vibrational energies is not considered. In reality, the levels become so close to each other that they form a quasi-continuum close to the dissociation limit. The role of energy transfer within this continuum is not well known and it would be interesting to investigate this in the future.

Nevertheless, we believe that the trends observed here give valuable information on the CO_2 conversion and on the vibrational excitation of CO_2 in a MW plasma. Our results indicate that the best conversion and energy efficiency are obtained at reduced pressure (i.e., around 300 mbar), in order to enhance vibrational-induced dissociation (mainly by reaction N1), since vibrational excitation is more effective at low pressures. This corresponds to important results obtained in literature[3,4]. Indeed, the best conversion and energy efficiency reported so far were obtained using a supersonic flow in a Laval nozzle[3,4]. According to our study, this supersonic flow can be beneficial for two reasons: (i) it creates a low pressure zone where vibrational excitation is more efficient and (ii) the gas temperature stays low, which prevents recombination upon increasing pressure, which we have seen to be particularly important in the afterglow. Indeed, our model predicts that low gas temperatures are beneficial for the vibrational excitation and thus enhance the non-equilibrium character of the plasma. Furthermore, this supersonic flow does not require a pumping system, which is also beneficial for the overall energy efficiency.

It is clear that enhancing the vibrational excitation can improve the energy efficiency. According to our model predictions, there are several ways to achieve this: using lower pressures, higher power densities (i.e. contracting the plasma) and reducing the gas temperature. Therefore, we believe that efforts should be made in designing more complex plasma discharges that manage to combine these properties, because conventional MW discharges operating at atmospheric pressure do not seem to take sufficient advantage of the non-equilibrium aspect of the plasma. As stated above, the Laval nozzle supersonic flow discharge seems very promising in that sense. Other paths are also being investigated, such as applying a vortex gas flow[16,42], which is thought to be beneficial for gas cooling.

Furthermore, pulsing the plasma power could also be beneficial for the conversion, as it prevents the gas from heating. More investigations in that direction are necessary. To summarize, this study shows that experiments do not systematically take advantage of the non-equilibrium aspect of the plasma and efforts should thus be made in that direction.

While this study was made for MW plasma discharges, we believe that the trends observed here are also valid for other types of plasmas, particularly gliding arc discharges, where vibrational excitation is also stated to be responsible for energy efficient CO_2 conversion[9,35].

Additionally, we would like to point out that, when comparing different CO_2 dissociation techniques, the extra energy costs of the whole installation should be taken into account. A blower would typically be needed, as well as a vacuum pump to work at low or intermediate pressures. A cooling system may also be required if the discharge produces too much heat. In experimental setups, the power consumed by a vacuum pump alone can be comparable to the plasma power, which makes it far from negligible. A study detailing the energy consumption of the different setups would be of great interest for potential industrial application of CO_2 dissociation.

4 Conclusion

We have used a zero-dimensional chemical kinetics model to describe the CO_2 conversion in a MW plasma. This model includes a detailed description of the vibrational kinetics of the asymmetric mode of CO_2 and the first levels of CO and O_2, as well as the energy transfers between these levels.

In a first step, we used a self-consistent gas temperature calculation to understand the effect of pressure and power density on the CO_2 conversion and energy efficiency, as well as the advantages of a faster cooling in the afterglow. Our model predicts that the conversion and energy efficiency reach a maximum of about 17% and 25%, respectively, between 300 and 400 mbar and with the standard power deposition profile (Figure 2, red curve). A higher power density has a beneficial effect on the conversion and energy efficiency at low pressure, which can reach up to 28% when the power deposition is 5 or 10 times denser, but almost no effect at high pressures. On the other hand, an increased cooling in the afterglow yields a higher conversion at 300 mbar and above, reaching up to 22% conversion, at 32% energy efficiency, at 500 mbar. The effect of cooling is particularly important at high pressure, when recombination plays a major role, while it is negligible at low pressure due to the little effect of recombination.

In a second step, we used the model to investigate the individual effect of power density, pressure and gas temperature on the vibrational distribution function of CO_2, and on the most important dissociation and recombination mechanisms, and we made a link between both, by determining the relative contribution of the individual vibrational levels to the overall dissociation.

The model predicts a larger vibrational excitation with increasing power deposition density and with decreasing pressure and temperature. A higher power deposition gives a higher electron density, which in turn enhances the transfer of electron energy to vibrational excitation. On the other hand, a higher pressure enhances the VT relaxation processes, so that the vibrational energy is lost again more quickly. Finally, the gas temperature was also identified as a key parameter. A higher gas temperature

also results in more pronounced VT transfers, making the vibrational levels thermalize faster. It is clear that we should exploit the strong non-equilibrium character of the MW plasma, with a pronounced vibrational excitation, as the latter is important for energy efficient CO_2 conversion. To realize this, it would be most beneficial to operate at reduced pressure, but still at sufficiently high power densities, while keeping the temperature under control.

We investigated the role of the most important dissociation and recombination mechanisms of CO_2, in the same range of operating conditions, i.e., power density, pressure and temperature. At low power densities, electron impact dissociation is the main dissociation mechanism, since the vibrational excitation is not significant enough to overcome the activation energy of the other dissociation reactions involving neutral species. At high power densities, the vibrational excitation is sufficient to overcome the activation energy of the neutral reactions that lead to dissociation of CO_2, i.e., upon collision with any neutral molecule or with O atoms (reactions N1 and N2 of Table S5 from the Supporting Information).

We also find that a higher gas temperature tends to favor the heavy particle dissociation reactions (N1 and N2), but the effect of the plasma-induced vibrational excitation becomes lower. Hence, a higher gas temperature is expected to be detrimental to the CO_2 conversion and energy efficiency. The same trend is observed with pressure: a higher pressure gives rise to more VT relaxation and is thus detrimental for the vibrational excitation. It is thus quite logical that a higher pressure reduces the CO_2 conversion and energy efficiency.

These observations help to explain the increase in conversion at low pressure. Indeed, an increase of power density has a positive effect on the vibrational excitation, especially at low pressure. This positive effect enhances in turn the dissociation through reactions N1 and N2, counterbalancing the importance of electron impact dissociation at low pressure. On the other hand, at high pressures, the gas tends to lose its vibrational excitation faster and the dissociation becomes more and more thermal. Therefore, the effect of the vibrational excitation is less important. The recombination reactions were also found to have an important effect at high gas temperatures and high pressures, especially in the afterglow. They are one of the main reasons of the decrease of conversion and energy efficiency at pressures close to atmospheric pressure. This explains why a higher cooling rate in the afterglow is particularly beneficial for the conversion and energy efficiency at high pressure.

In general, our model predicts that a higher pressure and gas temperature, especially in the afterglow, have a negative effect on the conversion and energy efficiency, while a higher power density is beneficial. These findings can explain the high energy efficiencies obtained with a supersonic gas flow, as the latter setup combines a reduced pressure and temperature with high power density.

The model provides interesting suggestions to enhance the CO_2 conversion and energy efficiency by identifying the limiting factors and how to take optimal advantage of the non-equilibrium in a MW discharge, either by applying a supersonic gas flow or a vortex flow, which leads to gas cooling, or by applying pulse power. Exploiting the non-equilibrium character of the MW plasma will increase the energy efficiency, which is crucial aspect for the application. The trends observed in this work are also valid more in general, for other types of discharges.

Supporting information

Reactions included in the models as well as their rate coefficients or cross sections.

5 Acknowledgements

We acknowledge financial support from the European Union's Seventh Framework Program for research, technological development and demonstration under grant agreement n° 606889. Furthermore, the research was also carried out in the framework of the Network on Physical Chemistry of Plasma-Surface Interactions - Interuniversity Attraction Poles, phase VII (PSI-IAP7), supported by the Belgian Science Policy Office (BELSPO). The calculations were carried out using the Turing HPC infrastructure at the CalcUA core facility of the Universiteit Antwerpen (UA), a division of the Flemish Supercomputer Center VSC, funded by the Hercules Foundation, the Flemish Government (department EWI) and the UA.

6 References

(1) IPCC 2013, Fifth Assesment Report: Climate Change 2013 Synthesis Report .

(2) Bogaerts, A.; Kozák, T.; van Laer, K.; Snoeckx, R. Plasma-Based Conversion of CO_2 : Current Status and Future Challenges. *Faraday Discuss.* **2015**, *183*, 217–232.

(3) Fridman, A. *Plasma Chemistry*; Cambridge University Press: New York, 2008.

(4) Asisov, R. I.; Vakar, A. K.; Jivotov, V. K.; Krotov, M. F.; Zinoviev, O. A.; Potapkin, B. V; Rusanov, A. A.; Rusanov, V. D.; Fridman, A. A. Non-Equilibrium Plasma-Chemical Process of CO_2 Decomposition in a Supersonic Microwave Discharge. *Proc. USSR Acad. Sci.* **1983**, *271* (1).

(5) Ramakers, M.; Michielsen, I.; Aerts, R.; Meynen, V.; Bogaerts, A. Effect of Argon or Helium on the CO_2 Conversion in a Dielectric Barrier Discharge. *Plasma Process. Polym.* **2015**, *12* (8), 755–763.

(6) Mei, D.; Zhu, X.; He, Y.-L.; Yan, J. D.; Tu, X. Plasma-Assisted Conversion of CO_2 in a Dielectric Barrier Discharge Reactor: Understanding the Effect of Packing Materials. *Plasma Sources Sci. Technol.* **2015**, *24* (1), 15011–15021.

(7) Aerts, R.; Somers, W.; Bogaerts, A. Carbon Dioxide Splitting in a Dielectric Barrier Discharge Plasma: A Combined Experimental and Computational Study. *ChemSusChem* **2015**, *8* (4), 702–716.

(8) Paulussen, S.; Verheyde, B.; Tu, X.; De Bie, C.; Martens, T.; Petrovic, D.; Bogaerts, A.; Sels, B. Conversion of Carbon Dioxide to Value-Added Chemicals in Atmospheric Pressure Dielectric Barrier Discharges. *Plasma Sources Sci. Technol.* **2010**, *19* (3), 034015 1-6.

(9) Nunnally, T.; Gutsol, K.; Rabinovich, a; Fridman, a; Gutsol, a; Kemoun, a. Dissociation of CO_2 in a Low Current Gliding Arc Plasmatron. *J. Phys. D. Appl. Phys.* **2011**, *44* (27), 274009.

(10) Indarto, A.; Yang, D. R.; Choi, J. W.; Lee, H.; Song, H. K. Gliding Arc Plasma Processing of CO_2 Conversion. *J. Hazard. Mater.* **2007**, *146* (1–2), 309–315.

(11) Spencer, L. F. The Study of CO_2 Conversion in a Microwave Plasma / Catalyst System. PhD dissertation, The University of Michigan, 2012.

(12) Spencer, L. F.; Gallimore, A. D. Efficiency of CO_2 Dissociation in a Radio-Frequency Discharge. *Plasma Chem. Plasma Process.* **2011**, *31* (1), 79–89.

(13) Silva, T.; Britun, N.; Godfroid, T.; Snyders, R. Optical Characterization of a Microwave Pulsed Discharge Used for Dissociation of CO_2. *Plasma Sources Sci. Technol.* **2014**, *23* (2), 25009.

(14) Bongers, W. A.; Welzel, S.; Bekerom, D. C. M. Van Den; Frissen, G.; Rooij, G. J. Van; Goede, A. P. H.; Graswinckel, M. F.; Groen, P. W.; Harder, N. den; Heemert, B. van; et al. Developments in CO_2 Dissociation Using Non-Equilibrium Microwave Plasma Activation for Solar Fuels Energy Conversion. In *22nd International Symposium on Plasma Chemistry (Antwerp, Belgium)*; 2015.

(15) Goede, A. P. H.; Bongers, W. A; Graswinckel, M. G.; Sanden, R. M. C. . Van De; Martina, L.; Jochen, K.; Schulz, A.; Mathias, W. Production of Solar Fuels by CO_2 Plasmolysis. *3rd Eur. Energy Conf. Budapest* **2014**, *1005*, 1–5.

(16) Bongers, W.; Bouwmeester, H.; Wolf, B.; Peeters, F.; Welzel, S.; van den Bekerom, D.; den Harder, N.; Goede, A.; Graswinckel, M.; Groen, P. W.; et al. Plasma-Driven Dissociation of CO_2 for Fuel Synthesis. *Plasma Process. Polym.* **2016**, No. July, 1–8.

(17) Kozák, T.; Bogaerts, A. Splitting of CO_2 by Vibrational Excitation in Non-Equilibrium Plasmas: A Reaction Kinetics Model. *Plasma Sources Sci. Technol.* **2014**, *23* (4), 45004.

(18) Treanor, C. E.; Rich J. W.; Rehm R. G. Vibrational Relaxation of Anharmonic Oscillators with Exchange-Dominated Collisions. *J. Chem. Phys.* **1968**, *48* (4), 1798.

(19) Kozák, T.; Bogaerts, A. Evaluation of the Energy Efficiency of CO_2 Conversion in Microwave Discharges Using a Reaction Kinetics Model. *Plasma Sources Sci. Technol.* **2015**, *24* (1), 15024.

(20) Aerts, R.; Martens, T.; Bogaerts, A. Influence of Vibrational States on CO_2 Splitting by Dielectric Barrier Discharges. *J. Phys. Chem. C* **2012**, *116*, 23257–23273.

(21) Koelman, P.; Heijkers, S.; Tadayon Mousavi, S.; Graef, W.; Mihailova, D.; Kozak, T.; Bogaerts, A.; van Dijk, J. A Comprehensive Chemical Model for the Splitting of CO_2 in Non-Equilibrium Plasmas. *Plasma Process. Polym.* **2016**, 1–20.

(22) Ponduri, S.; Becker, M. M.; Welzel, S.; Van De Sanden, M. C. M.; Loffhagen, D.; Engeln, R. Fluid Modelling of CO_2 Dissociation in a Dielectric Barrier Discharge. *J. Appl. Phys.* **2016**, *119* (9).

(23) Heijkers, S.; Snoeckx, R.; Kozák, T.; Silva, T.; Godfroid, T.; Britun, N.; Snyders, R.; Bogaerts, A. CO_2 Conversion in a Microwave Plasma Reactor in the Presence of N_2 : Elucidating the Role of Vibrational Levels. *J. Phys. Chem. C* **2015**, *119* (23), 12815–12828.

(24) Bogaerts, A.; Wang, W.; Berthelot, A.; Guerra, V. Modeling Plasma-Based CO_2 Conversion : Crucial Role of the Dissociation Cross Section. *Plasma Sources Sci. Technol.* **2016**, *25*, 1–23.

(25) Grofulovic, M.; Alves, L. L.; Guerra, V. Electron-Neutral Scattering Cross Sections for CO_2: A Complete and Consistent Set and an Assessment of Dissociation. *J. Phys. D Appl. Phys.* **2016**, *49*, 395207.

(26) Phelps, A. V. Phelps Database Www.lxcat.net, Retrieved on December 4, 2015.

(27) Pietanza, L. D.; Colonna, G.; D'Ammando, G.; Laricchiuta, a; Capitelli, M. Vibrational Excitation and Dissociation Mechanisms of CO_2 under Non-Equilibrium Discharge and Post-Discharge Conditions. *Plasma Sources Sci. Technol.* **2015**, *24* (4), 42002.

(28) Pietanza, L. D.; Colonna, G.; D'Ammando, G.; Laricchiuta, A.; Capitelli, M. Electron Energy Distribution Functions and Fractional Power Transfer In "cold" and Excited CO_2 Discharge and Post Discharge Conditions. *Phys. Plasmas* **2016**, *23* (1).

(29) Pietanza, L. D.; Colonna, G.; D'Ammando, G.; Laricchiuta, A.; Capitelli, M. Non Equilibrium Vibrational Assisted Dissociation and Ionization Mechanisms in Cold CO_2 Plasmas. *Chem. Phys.* **2016**, *468*, 44–52.

(30) Pancheshnyi, S.; Eismann, B.; Hagelaar, G. J. M.; Pitchford, L. C. *Comput. code ZDPlasKin http//www.zdplaskin.laplace.univ-tlse.fr (University Toulouse, LAPLACE, CNRS-UPS-INP, Toulouse, Fr. 2008).*

(31) Schluter, H.; Shivarova, A. Travelling-Wave-Sustained Discharges. *Phys. Rep.* **2007**, *443* (4–6), 121–255.

(32) Hagelaar, G. J. M.; Pitchford, L. C. Solving the Boltzmann Equation to Obtain Electron Transport Coefficients and Rate Coefficients for Fluid Models. *Plasma Sources Sci. Technol.* **2005**, *14* (4), 722–733.

(33) Berthelot, A.; Bogaerts, A. Modeling of Plasma-Based CO_2 Conversion: Lumping of the Vibrational Levels. *Plasma Sources Sci. Technol.* **2016**, *25* (4), 45022.

(34) Guerra, V.; Tatarova, E.; Dias, F. M.; Ferreira, C. M. On the Self-Consistent Modeling of a Traveling Wave Sustained Nitrogen Discharge. *J. Appl. Phys.* **2002**, *91* (5), 2648–2661.

(35) Wang, W.; Berthelot, A.; Kolev, S.; Tu, X.; Bogaerts, A. CO_2 Conversion in a Gliding Arc Plasma: 1D Cylindrical Discharge Model. *Plasma Sources Sci. Technol.* **2016**, *25* (6), 65012.

(36) Pietanza, L. D.; Colonna, G.; Laporta, V.; Celiberto, R.; D'Ammando, G.; Laricchiuta, A.; Capitelli, M. Influence of Electron Molecule Resonant Vibrational Collisions over the Symmetric Mode and Direct Excitation-Dissociation Cross Sections of CO_2 on the Electron Energy Distribution Function and Dissociation Mechanisms in Cold Pure CO_2 Plasmas. *J. Phys. Chem. A* **2016**, *120* (17), 2614–2628.

(37) Pietanza, L. D.; Colonna, G.; D'Ammando, G.; Capitelli, M. Time-Dependent Coupling of Electron Energy Distribution Function, Vibrational Kinetics of the Asymmetric Mode of CO_2 and Dissociation, Ionization and Electronic Excitation Kinetics under Discharge and Post-Discharge Conditions. *Plasma Phys. Control. Fusion* **2017**, *59* (1), 14035.

(38) Suzuki, I. General Anharmonic Force Constants of Carbon Dioxide. *J. Mol. Spectrosc.* **1968**, *25* (4), 479–500.

(39) Huber, K.; Herzberg, G. Constants of diatomic molecules http://webbook.nist.gov/.

(40) Lawton, S. a.; Phelps, A. V. Excitation of the $b^1\Sigma^+_g$ State of O_2 by Low Energy Electrons. *J. Chem. Phys.* **1978**, *69* (3), 1055–1068.

(41) den Harder, N.; van den Bekerom, D. C. M.; Al, R. S.; Graswinckel, M. F.; Palomares, J. M.; Peeters, F. J. J.; Ponduri, S.; Minea, T.; Bongers, W. A.; van de Sanden, M. C. M.; et al. Homogeneous CO_2 Conversion by Microwave Plasma: Wave Propagation and Diagnostics. *Plasma Process. Polym.* **2016**, No. July, 1–24.

(42) Harder, N. den. From Temperature to Reactivity: Optical Diagnosis of High-Density Plasmas. PhD Dissertation, Technical University of Eindhoven 2016.